JACS JOURNAL OF THE AMERICAN CHEMICAL SOCIETY

Article

Cite This: J. Am. Chem. Soc. 2019, 141, 10770−10776

pubs.acs.org/JACS

A Transient and Flexible Cation−π Interaction Promotes Hydrolysis of Nucleic Acids in DNA and RNA Nucleases

Vito Genna,[†] Marco Marcia,[‡] and Marco De Vivo*[,†]

[†]Laboratory of Molecular Modeling and Drug Discovery, Istituto Italiano di Tecnologia, Via Morego 30, 16163, Genoa, Italy

[‡]European Molecular Biology Laboratory (EMBL) Grenoble, 71 Avenue des Martyrs, Grenoble 38042, France

Supporting Information

ABSTRACT: Metal-dependent DNA and RNA nucleases are enzymes that cleave nucleic acids with great efficiency and precision. These enzyme-mediated hydrolytic reactions are fundamental for the replication, repair, and storage of genetic information within the cell. Here, extensive classical and quantum-based free-energy molecular simulations show that a cation−π interaction is transiently formed *in situ* at the metal core of Bacteriophage−λ Exonuclease (Exo−λ), during catalysis. This noncovalent interaction (Lys131−Tyr154) triggers nucleophile activation for nucleotide excision. Then, our simulations also show the oscillatory dynamics and swinging of the newly formed cation−π dyad, whose conformational change may favor proton release from the cationic Lys131 to the bulk solution, thus restoring the precatalytic protonation state in Exo−λ. Altogether, we report on the novel mechanistic character of cation−π interactions for catalysis. Structural and bioinformatic analyses support that flexible orientation and transient formation of mobile cation−π interactions may represent a common catalytic strategy to promote nucleic acid hydrolysis in DNA and RNA nucleases.

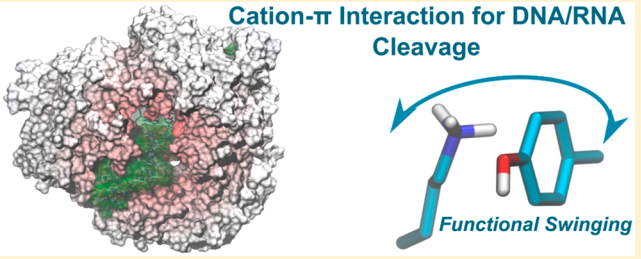

INTRODUCTION

Nucleic acid hydrolysis controls vital processes, including the maintenance of chromatin integrity and large-scale genome stability as well as aging and cell defense.[1,2] This chemical reaction is efficiently performed by a large set of pharmaceutically relevant enzymes, which includes topoisomerases, recombinases, ribozymes, and DNA/RNA nucleases.[3−5] While exonucleases hydrolyze the 5′-end strand of the nucleic acid substrate, endonucleases cleave a phosphodiester bond within a polynucleotide strand.[6−8] Regardless of their cleavage point, both exo- and endonucleases catalyze the S_N2-type phosphoryl transfer, mostly via the recognized two-metal-ion mechanism.[9−15] This hydrolytic reaction requires deprotonation of the nucleophilic oxygen, followed by the nucleophilic attack of the latter on the scissile phosphate group of the dsDNA substrate.[16−18] This nucleophilic reaction leads to the cleavage of the P−O3′ bond, and the concomitant generation of the free 5′-phosphate nucleotide and 3′-OH products.

Thus, the phosphoryl-transfer reaction occurs while the nucleophile sits on the 3′-end side of the phosphodiester group, properly positioned for the in-line nucleophilic attack on the scissile phosphate group (Figure 1).[17,21] Notably, the catalytic center is surrounded by conserved second-shell basic residues (i.e., Arg and Lys), which were recently identified in a large set of nucleic-acid-processing enzymes (including nucleases). It has been suggested that these residues are critical for the formation of a precatalytic Michaelis−Menten complex.[22−29]

In this context, recent data have revealed that the presence of a second-shell basic residue, Lys131, is critical in promoting catalysis in Bacteriophage−λ Exonuclease (Exo−λ, a representative and well-characterized member of the type II restriction endonuclease-like superfamily).[19,20] Lys131 extends into the Exo−λ active site to form ion pairs with the *pro*-S_p atom of the scissile phosphate. Concomitantly, it forms a long-range attractive electrostatic interaction with the *pro*-R_p atom (at 3.89 Å) of the neighboring 3′-phosphate.[18] This contact framework also involves the aromatic side chain of the neighboring Tyr154; a residue that closes over the active site through an H-bond established with the DNA backbone (Figure 1). Intriguingly, Lys131 has been postulated to activate (i.e., deprotonate) the nucleophilic water that triggers the S_N2-type phosphoryl transfer for dsDNA hydrolysis. Also, Tyr154 has been noted to form hydrogen bond interactions with the neighboring 3′ phosphate.[19,20] Nevertheless, despite the wealth of experimental and structural data on Exo−λ,[19,20] the chemical steps for activation and catalysis at this enzyme's active core are still unclear.

Here, we tackle this challenge with a series of microsecond-scale force-field-based (FF) molecular dynamics (MD) simulations and free-energy calculations via the hybrid Car−Parrinello quantum mechanics/molecular mechanics (CP QM/MM) approach.[30−32] We describe a novel chemical mechanism where Lys131 acts in tandem with Tyr154 to

Received: April 12, 2019
Published: June 18, 2019

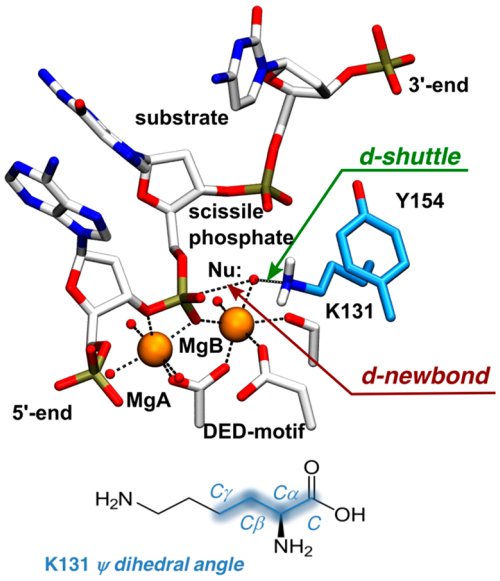

Figure 1. Precatalytic state of Bacteriophage-λ Exonuclease (Exo-λ) binary complex, built from PDBid 4WUZ[19] and 3SM4.[20] Cation−π-interacting amino acids (Lys131 and Tyr154) are reported in blue. Orange spheres identify catalytic Mg^{2+} ions. The red arrow indicates the forming bond (*d-newbond*). The green arrow indicates the reaction coordinate describing the deprotonation event (*d-shuttle*).

transiently generate a cation−π interaction to promote the Exo−λ-mediated S_N2-type phosphoryl-transfer reaction for dsDNA hydrolysis.

We found that Lys131 is deprotonated in the reactant state, as already shown for analogous lysine residues in other enzymes.[33−35] Thus, Lys131 can act as a general base and accept a proton from the Mg-oriented nucleophilic water molecule within the catalytic site of Exo−λ. In this way, a cation−π interaction is formed by Lys131 and Tyr154. We observed that, once this cation−π interaction is formed, these paired amino acid side chains swing jointly out of the catalytic site. This may allow the cationic Lys131 to release one proton in solution, thus closing the Exo−λ catalytic turnover (Figure 2). Finally, thanks to extensive structural and bioinformatics analyses, we show that formation of a catalytically active cation−π interaction might be a general strategy used by several other viral and bacterial nucleases.

RESULTS AND DISCUSSION

Role of Lys131 from Force-Field-Based MD Simulations. First, we investigated the binary Exo-λ/dsDNA complex using extensive FF-based MD simulations (~3.5 μs overall). Initially, we considered two systems where Lys131 is either protonated or in its neutral state. In particular, we monitored the evolution over time of three geometrical descriptors:[16,36] (*i*) the length of the forming bond between the phosphorus of the scissile phosphate and the nucleophilic

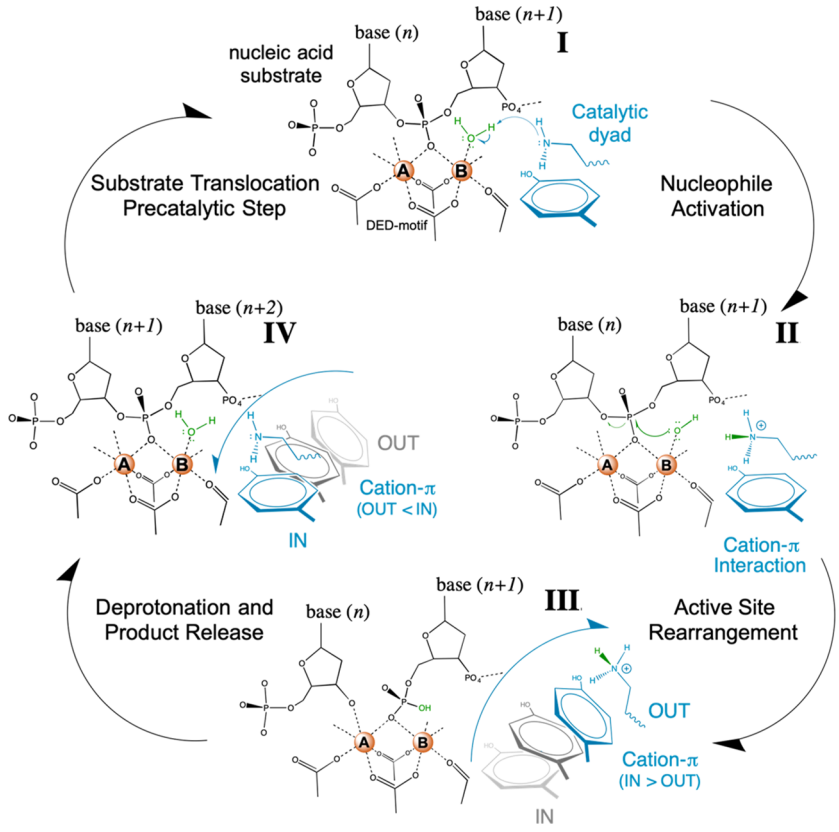

Figure 2. General reaction scheme proposed for cation−π−mediated dsDNA hydrolysis operated by Exo-λ. The flexible cation−π interaction is shown in blue. (**I**) Precatalytic complex where the nucleophile activation step occurs. (**II**) After nucleophile activation, the Lys131-Tyr154 dyad generates the cation−π interaction. (**III**) Rearrangement and oscillatory dynamics of the cation−π system leading to the synchronous departure of the Lys131-Tyr154 pair from the core of the catalytic center. At this point, Lys131 deprotonation may occur, with subsequent product release. The newly formed neutral dyad can readjust into the active site to reconstitute the competent precatalytic architecture and start a new catalytic cycle (**IV**).

DOI: 10.1021/jacs.9b03663
J. Am. Chem. Soc. 2019, 141, 10770−10776

water molecule, "*d-newbond*"; (*ii*) the distance between the nitrogen atoms of Lys131 and the oxygen atom of the attacking water, "*d-shuttle*"; and (*iii*) the ψ dihedral angle formed by the atoms $C-C_{\alpha}-C_{\beta}-C_{\gamma}$ of Lys131. This angle is a good depiction of the residue position with respect to the Exo-λ active core (Figure 1).

Our MD simulations show that the protonated Lys131 escapes its crystallographic pose after only ~250 ns (Figure S1). This is shown by *d-shuttle* and ψ values, which move from 2.8 ± 0.6 Å to 7.8 ± 1.2 Å and from −168° ± 22.5° to 80° ± 9.6°, respectively (Figures 3 and S1). This Lys131 structural

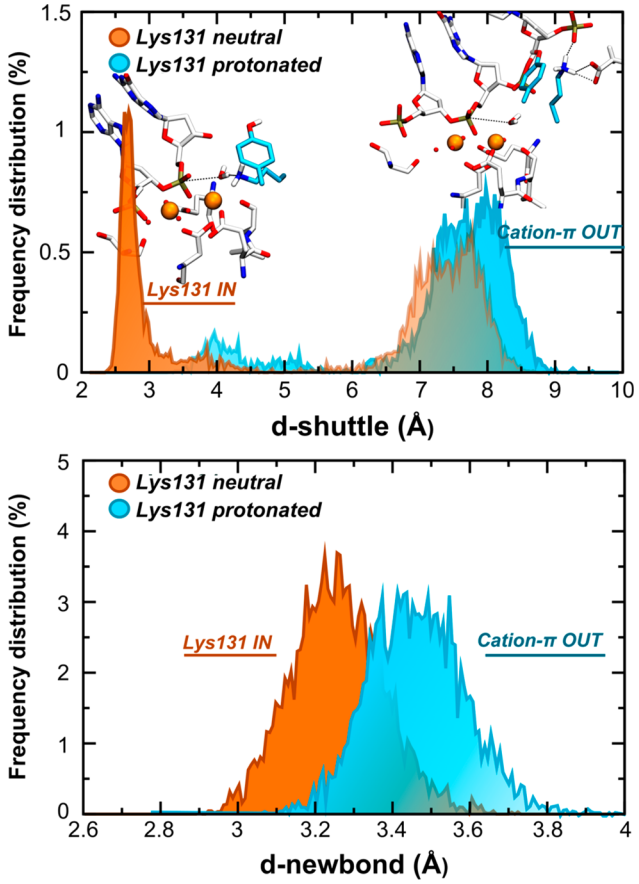

Figure 3. Exo-λ precatalytic state dynamics. The system with neutral Lys131 is in orange. The system with the protonated form is in cyan. (Upper graph) Frequency distribution of *d-shuttle* (i.e., N@Lys131-O@Wat). (Lower graph) Frequency distribution of d-newbond (i.e., O@Wat-P) in both systems.

rearrangement causes the breaking of the native H-bond network on top of Mg_B, with the inactivated nucleophilic water molecule that consequently shifts ±0.6 Å away from the scissile phosphorus when compared to the X-ray structure (3.7 ± 0.25 Å in MD vs 3.1 Å in PDBid 3SM4).[19,20] Thus, the reagents are no longer positioned for optimal in-line nucleophilic attack (Figure S2), with the shifting of the nucleophile that is mainly induced by the cationic Lys131−NH_3^+ group, which alters the native coordination geometry of Mg_B.

Notably, in our MD simulations, the protonated Lys131 moves out of the active site after generating the cation−π interaction with the neighboring phenolic hydroxyl group of Tyr154. Formation of this cation−π interaction is primarily driven by the electrostatics and van der Waals contacts between the electron-rich aromatic group of Tyr154 and the electron-deficient cationic Lys131.[37,38] This noncovalent interaction is known to alleviate the positive charge of the Lys131−NH_3^+ group, thanks to the presence of a partial negative charge residing in the electron-rich π-system of the Tyr154 hydroxyphenyl moiety.[39−42] Once the cation−π interaction is formed (Figure 2, step III), the positively charged Lys131 establishes an ionic contact with the phosphate group of the nucleotide located on the 3′-side of the scissile phosphate, and it becomes partially solvent-exposed (Figure S3). After an additional ~150 ns, the Lys131 side chain swings out completely from the active site and becomes fully solvent-exposed. Here, *d-shuttle* and ψ adopt values of 7.8 ± 0.8 Å and 85° ± 18°, respectively. Also, *d-newbond* increases from its crystallographic value (i.e., 3.2 Å, PDBid 3SM4)[20] to stably adopt a value of 3.6 ± 0.2 Å. These values are stably maintained for the ±1.5 μs successive MD trajectory (Figure 3 and Figure S1). Importantly, while the cation−π system progressively abandons the active site, the hydroxyl moiety of Tyr154 establishes an ionic interaction with the dsDNA backbone (Figure S3).

This Tyr154 interaction further locks the solvent exposed position of Lys131. This likely facilitates its deprotonation step. Here, the new electrostatic field surrounding Lys131 is defined by the nearby hydrophobic amino acids Pro133, Phe142, Phe172 and by hydrophobic moieties of the backbone of the substrate (i.e., ribose of dC3). This environment lowers the pK_a of Lys131 by two units (from ~10.5 to 8.4, see below), likely favoring proton release.[43] Notably, drops in pK_a values (as low as 5.3) have been experimentally reported for Lys residues buried within the enzymes' core.[44] In this "out" conformation, Lys131 occasionally interacts with either the conserved Asp138 or with a phosphate group located on the 3′-side of the scissile phosphate (Figure S3). These negatively charged residues may thus favor proton release from the Lys−NH_3^+ group, acting as a final proton acceptor, as observed in other enzymes (see calculations below on pK_a estimates and energetics of proton release, as well as structural analyses of the protein surrounding of Lys131, when in "out" conformations).[45−49] Notably, if deprotonated, Lys131 starts to swing, adopting "in" and "out" conformations, thus restoring the initial precatalytic conditions (Figure 2). We also simulated the Tyr154Ala mutated system (~500 ns). Here, we observed that the lack of Tyr154, and in turn Lys131 stabilization via formation of the Lys131-Tyr154 dyad, leads to structural instability of the catalytic site. This is well visible by the deviation (~5 Å apart) of the two catalytic Mg ions, along with the misalignment of the nucleophile (Supporting Figure S4). Consequently, the active site adopts an architecture that is significantly distorted (and likely not reactive) with respect to the one observed in the prereactive X-ray structure of Exo-λ.[19]

In contrast, the 1.5-μs-long MD simulations of the system with Lys131 in its neutral state (i.e., $-NH_2$) returned an active site architecture that maintained the precise interaction framework of the crystallographic structures used to build our system (Figure S5). Indeed, *d-shuttle* rests at a value of 2.8 ± 0.8 Å (Figure 3), which is in a distance range typical of a stable H-bond interaction. Here, Ψ also maintains the native value of −165° ± 21° detected in the nonreactive X-ray structure (PDBid 4WUZ).[19] *d-newbond* shows a value of 3.2 ± 0.7 Å (Figure 3), which finely matches the crystallographic value of 3.2 Å (PDBid 3SM4).[20] Lastly, both the nucleophilic

DOI: 10.1021/jacs.9b03663
J. Am. Chem. Soc. 2019, 141, 10770−10776

water molecule and Tyr154 keep their native position as in the starting X-ray structure (Figure S5).[19,20]

The residues involved in the formation of a cation−π interaction may experience two distinct and opposite electrostatic forces.[39,40,50] On the one hand, the neutral alkyl side chain of Lys131 may be repulsed by the electron-rich π-system of Tyr154. In Exo−λ, based on our simulations, this repulsion seems to favor the formation of the H-bond interaction between the deprotonated Lys131 and the nucleophilic water molecule in the competent precatalytic state. On the other hand, once the Lys131 abstracts the proton from the nucleophile, it is attracted by the electron-rich ring of Tyr154, giving rise to the transient cation−π interaction that promotes catalysis by activating the nucleophilic water.

In our MD simulations, the Lys131-Tyr154 dyad shows an oscillatory dynamic (like a pendulum), which is likely to favor the release of the abstracted proton to a final acceptor located outside of the inner coordination shell of the bimetallic active core. In this way, Lys131 becomes transiently protonated and finally neutral to restore the reactant state. Therefore, our MD results suggest a possible catalytic mechanism, in which the formation of a cation−π interaction (Tyr154-Lys131) is used to (*i*) trigger the activation (i.e., deprotonation) of the nucleophile through the initially neutral Lys131, which, once protonated, forms a cation−π interaction with Tyr154; and (*ii*) help proton release to the bulk solution via the swinging of the newly formed cation−π dyad, which is likely further aided by the Lys131 contacts with the conserved Asp138, or with the phosphate group located on the 3′-side of the scissile phosphate; (*iii*) Finally, after proton release, the deprotonated Lys131 can return to its original position (i.e., the crystallographic one) to start a new round of catalysis (Figure 2). This three-step mechanism comprises nucleophile activation, nucleotide cleavage, and proton release, with regeneration of the prereactive state after substrate translocation. These steps form a closed-loop cycle for Exo-λ-mediated dsDNA hydrolysis (Figure 2).

QM/MM Simulations of Nucleophile Activation in Exo-λ Catalysis. To corroborate this mechanistic hypothesis and define its dynamics and semiquantitative energetics, we explicitly considered the electronic effects in the Lys131-Tyr54 dyad's catalytic role in the nucleophile activation and dsDNA hydrolysis in Exo-λ. Thus, we performed ab initio CP QM/MM simulations coupled with metadynamics-based free-energy calculations, aware of the limitations of such an approach in fully accounting for dispersion and van der Waals forces involved in cation−π interactions.[37,51,52]

First, we used two collective variables (CV1 and CV2; see Supporting Information for further details) to investigate the in-line proton transfer for the *in situ* formation of the catalytically active 3′-hydroxide ion, along with the S_N2-type reaction for nucleotide cleavage. CV1 is defined as the difference between the lengths of the breaking O_{wat}−H_{wat} bond (i.e., *r1*) and forming H_{wat}−Lys bond (i.e., *r2*, Figure 4A). CV2 is the difference between the breaking phosphodiester bond P−3′O (i.e., *r3*) and forming O_{wat}−P bonds (i.e., *r4*, Figure 4A). The free-energy surface (FES), projected on these CVs, shows that DNA hydrolysis in Exo-λ occurs through a stepwise mechanism (Figure 4C). Indeed, as shown by the FES profile, the proton transfer for nucleophile activation (i.e., Lys131 protonation) and the S_N2-type phosphoryl-transfer reaction are asynchronous chemical events (CV1 and CV2).

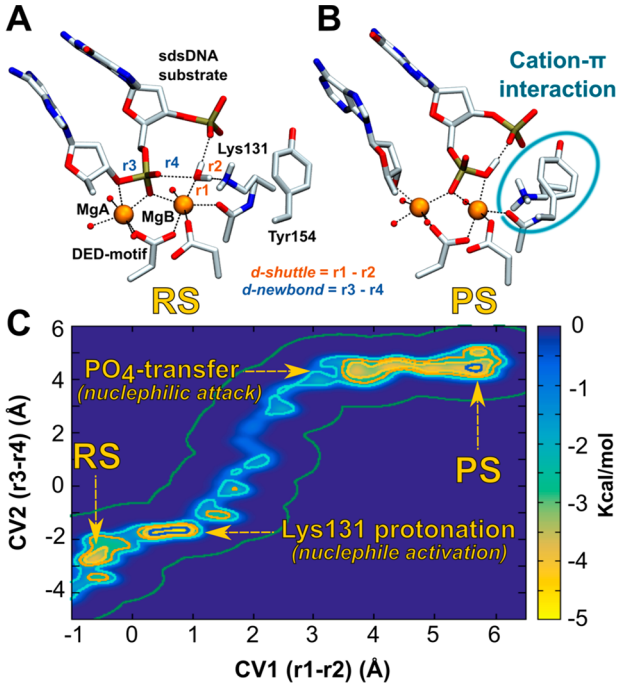

Figure 4. Structural details for the cation−π-mediated DNA hydrolysis in Exo-λ, as in Figure 2. (A) RS indicates the reactant state. (B) PS indicates the products state, with the cation−π just formed, in the IN orientation. (C) Free-energy surface and reaction path from global minima in RS (point I, Figure 2) to PS (point IV, Figure 2).

Our starting system is initially located in a stable minimum (i.e., RS point on the FES reported in Figure 4), with a free energy of ∼ −5 kcal/mol. Here, *d-shuttle* and *d-newbond* have a value of ∼3.2 Å and ∼3.3 Å, thus finely reproducing the crystallographic values (in PDBid 3SM4).[20] From this point, the system evolves toward a second local minimum located at CV1 ≈ −0.8 Å and CV2 ≈ −2.1 Å, where the phosphoryl transfer reaction occurs. Indeed, the increase of CV1 (dictated by the increasing of *r1* and the concomitant shortening of *r2*) marks the end of the in-line proton transfer with the consequent *in situ* formation of the nucleophilic species (i.e., OH^-).

Here, the protonation of Lys131 leads to the formation of the cation−π interaction with Tyr154 (i.e., the catalytic dyad). Once the attacking OH^- group has been formed, the system further proceeds toward the products, overcoming an energetic barrier of ∼4.5 kcal/mol. Although qualitative, we note that the computed free energy is in excellent agreement with the experimentally measured barrier of 5.3 kcal/mol, obtained from single-molecule kinetics assays and steady-state kinetics studies.[53,54] Finally, complete products formation occurs in a free-energy basin located at CV1 ≈ −3.5 Å and CV2 ≈ −4 Å.

Nonetheless, Exo-λ further explores the free-energy surface to reach a more stable conformational state in a deeper energy well, which is located at CV1 ≈ −6 Å and CV2 ≈ −4.5 Å. Here, the energy value is again ∼ −5 kcal/mol and, as shown by the increase in CV1 with respect to the previous metastable point, the Lys131-Tyr154 dyad is now ∼6 Å away from the catalytic site (i.e., PS point on the FES reported in Figure 4).

We also evaluated the energetics for the deprotonation of Lys131 via a second set of *ab initio* hybrid QM/MM simulations coupled to umbrella sampling.[30,55,56] We com-

DOI: 10.1021/jacs.9b03663
J. Am. Chem. Soc. 2019, 141, 10770−10776

puted the in-line proton transfer from the protonated Lys131 to either the conserved Asp138 or a bulk water molecule. In both cases, the proton transfer event is described along a reaction coordinate (RC) defined by the difference between the length of the breaking $N_{Lys}-H_{Lys}$ (i.e., r1) and forming $H_{Lys}-O_{Wat}$ bonds (i.e., r2, Figure 5). Proton transfer occurs

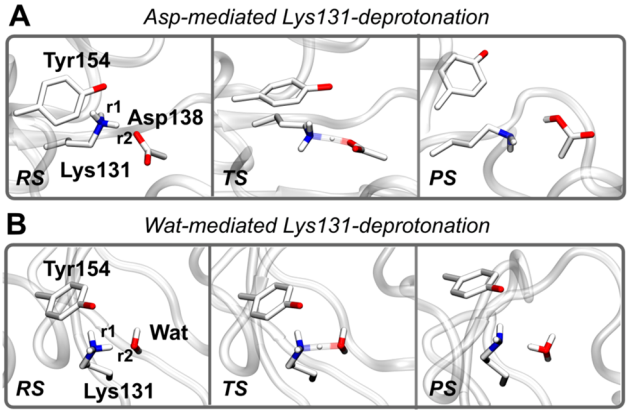

Figure 5. Snapshots along the QM/MM simulations performed to estimate the energetics for two possible deprotonation mechanisms of Lys131 in Exo-λ (A and B). (A) Proton transfer from Lys131 to Asp138. (B) Proton transfer from Lys131 to a water molecule. RS indicates the reactant state and TS the transition state, while PS indicates the products state. Notably, in both PS states, the cation$-\pi$ interaction is lost, with consequent visible disruption of the Lys131-Tyr154 dyad.

with an energy barrier of 6.5 ± 1.6 kcal/mol (to Asp138) and 6.2 ± 1.4 (to water) (Figure S6). Notably, once the proton has been completely transferred to the acceptor, the cation$-\pi$ interaction is broken and Tyr154 starts to move away from the deprotonated Lys131. No spontaneous Lys131 reprotonation event, after proton migration, is observed in unconstrained simulations. In addition, Lys131 deprotonation is also supported by its reduced pK_a value when in "out" conformations, with respect to the inward ones. Indeed, after computing the side chain pK_a value of Lys131 through continuum electrostatics calculations based on the nonlinear Poisson–Boltzmann equation (DelPhiPKa)[57,58]—applied to ~20 snapshots extracted by both classical and QM/MM MD simulations—we have observed a drop of ~2 units in the pK_a value of Lys131, passing from the computed value of 10.4 ± 0.5 ("in" conformations), to 8.4 ± 0.5 ("out" conformations). Such a pK_a drop is likely due to the location in the "out" conformations of Lys131, which is surrounded by hydrophobic residues, i.e. Pro133, Phe142, Tyr154, and Phe172. These hydrophobic pockets typically lower the pK_a of lysines.[43,44] Together, these results and observations corroborate the possibility that "out" conformations of Lys131 favor its deprotonation, and likely product release as well as nucleophile selection for Exo-λ exonuclease activity.

These quantum simulations confirm our classical MD-based mechanistic hypothesis. While, from our simulations, it would be a stretch to indicate the rate-determining step for such a multistep catalytic reaction mechanism (phosphoryl transfer and Lys131 deprotonation are nearly isoenergetic, from our computed values), our results suggest that mutation of Tyr154 in Exo-λ with alternative aromatic residues may lead to different interaction energies with the cationic counterpart,[39,59,60] likely yielding different Exo-λ catalytic rates and efficiencies. This may indicate a strategy for obtaining a tunable site and molecular switch in order to regulate nuclease-mediated nucleic acid hydrolysis in Exo-λ.

Similarities with Other Nucleases. On the basis of our findings, we investigated whether this chemical strategy is used by other nucleases. We noticed that Lys131 is strictly conserved in exonucleases from at least 10 Exo-λ of different species. It occupies a critical position, well-suited to a catalytic role, in a multitude of phosphodiester-bond-processing enzymes, including *Haemophilus influenzae*, *Vibrio Phage 2E1*, and *Cronobacter Phage ENT47670* (Figure S7).[23] Similarly, Tyr154 is invariantly present in exonucleases,[23] suggesting that the proposed mechanism may be extended to several other exonucleases. Moreover, we performed structural and bioinformatics comparisons between Exo-λ and selected endonucleases. Indeed, potential correlations have been detected in enzymes where such a cation$-\pi$ interaction seems to be present and conserved, like in *Bam*HI (Lys131 → Lys61 and Tyr154 → Phe112), *PvuII* (Lys131 → Lys70 and Tyr154 → Trp99), and *RNase H* (Lys131 → Lys138 and Tyr154 → Tyr163). Likewise, a catalytic cation$-\pi$ interaction could be used in phage *T4 endonuclease VII* (PDBid: 2QNC),[61] where the essential His41/43 (part of a proton-shuttling histidine triad, His43-His41-His105) might act as a general base for nucleophile activation (i.e., deprotonation of a water molecule). Indeed, if this is the case, then the histidine triad might operate as a proton-transporter chain, as shown for *human histidine triad nucleotide binding protein 1*.[62] Here, the neighboring π-system (represented by Tyr8) might mitigate the positive charge on His105 by establishing a cation$-\pi$ interaction (Figure S8).

Similarly, based on the parallelism between the active site architecture and reaction mechanism between *T4 endonuclease VII*, *Vibrio vulnificus nuclease*, and *Cas9 endonuclease*,[63−65] an analogous hypothesis could also be proposed for Cas9 catalysis. Indeed, as recently reported,[23,66−69] the positively charged and functionally relevant Lys974/976 residues in *Cas9 nuclease* (PDBid 5Y36)[70,71] mimic Lys131, and also the analogous (and catalytic) His43 and Arg99 found in *T4 endonuclease VII* and *Vibrio vulnificus nuclease*, respectively.[63] The counterpart of these positively charged residues in *Cas9* are likely to be the structurally conserved His982/983, or Tyr1272.[67−69] Altogether, these structural observations further corroborate our proposed mechanism of a functional cation$-\pi$ interaction for nuclease enzymatic activity.

■ CONCLUSIONS

In summary, we propose a new mechanism for phosphodiester bond hydrolysis in nuclease enzymes. This mechanism exploits the oscillatory dynamics of a transiently formed cation$-\pi$ interaction, which in turn promotes efficient nucleic acid hydrolysis. Thus, our work proposes a conceptually novel enzymatic strategy for the proton-abstracting general base (and proton release) in the active site of endo- and exonucleases.[6,19,20] This may help in developing tunable artificial enzymes for nucleic acid processing,[72] as well as new ways to modulate catalysis in pharmaceutically relevant nucleases.

■ ASSOCIATED CONTENT

Supporting Information

The Supporting Information is available free of charge on the ACS Publications website at DOI: 10.1021/jacs.9b03663.

DOI: 10.1021/jacs.9b03663
J. Am. Chem. Soc. 2019, 141, 10770−10776

Setup protocols on classical and CP QM/MM simulations and additional analyses; PDB analyses and sequence alignments in supplementary Figures S1−S8 (PDF)

AUTHOR INFORMATION

Corresponding Author

*marco.devivo@iit.it

ORCID

Vito Genna: 0000-0002-4664-8086

Marco Marcia: 0000-0003-2430-0713

Marco De Vivo: 0000-0003-4022-5661

Notes

The authors declare no competing financial interest.

ACKNOWLEDGMENTS

V.G. thanks the European Molecular Biology Organization (EMBO) for financial support (ALTF 103-2018). Work in the Marcia lab is partly funded by the Agence Nationale de la Recherche (ANR-15-CE11-0003-01), by the Agence Nationale de Recherche sur le Sida et les hépatites virales (ANRS) (ECTZ18552), and by ITMO Cancer (18CN047-00). The Marcia lab uses the platforms of the Grenoble Instruct Center (ISBG: UMS 3518 CNRS-CEA-UJF-EMBL) with support from FRISBI (ANR-10-INSB-05-02) and GRAL (ANR-10-LABX-49-01) within the Grenoble Partnership for Structural Biology (PSB). M.D.V. thanks the Italian Association for Cancer Research (AIRC) for financial support (IG 18883). We thank Grace Fox for proofreading and copyediting the manuscript.

REFERENCES

(1) Sancar, A. Mechanisms of DNA Repair by Photolyase and Excision Nuclease (Nobel Lecture). *Angew. Chem., Int. Ed.* **2016**, *55*, 8502−8527.

(2) Dewar, J. M.; Lydall, D. Pif1- and Exo1-dependent nucleases coordinate checkpoint activation following telomere uncapping. *EMBO J.* **2010**, *29*, 4020−4034.

(3) Sakuma, T.; Woltjen, K. Nuclease-mediated genome editing: At the front-line of functional genomics technology. *Dev. Growth Differ.* **2014**, *56*, 2−13.

(4) Keyel, P. A. Dnases in health and disease. *Dev. Biol.* **2017**, *429*, 1−11.

(5) Riccardi, L.; Genna, V.; De Vivo, M. Metal-ligand interactions in drug design. *Nat. Rev. Chem.* **2018**, *2*, 100−112.

(6) Yang, W. Nucleases: diversity of structure, function and mechanism. *Q. Rev. Biophys.* **2011**, *44*, 1−93.

(7) Pingoud, A.; Fuxreiter, M.; Pingoud, V.; Wende, W. Type II restriction endonucleases: structure and mechanism. *Cell. Mol. Life Sci.* **2005**, *62*, 685−707.

(8) Galburt, E. A.; Stoddard, B. L. Catalytic mechanisms of restriction and homing endonucleases. *Biochemistry* **2002**, *41*, 13851−13860.

(9) Palermo, G.; Cavalli, A.; Klein, M. L.; Alfonso-Prieto, M.; Dal Peraro, M.; De Vivo, M. Catalytic metal ions and enzymatic processing of DNA and RNA. *Acc. Chem. Res.* **2015**, *48*, 220−228.

(10) Ho, M. H.; De Vivo, M.; Dal Peraro, M.; Klein, M. L. Understanding the effect of magnesium ion concentration on the catalytic activity of ribonuclease H through computation: does a third metal binding site modulate endonuclease catalysis? *J. Am. Chem. Soc.* **2010**, *132*, 13702−13712.

(11) De Vivo, M.; Dal Peraro, M.; Klein, M. L. Phosphodiester cleavage in ribonuclease H occurs via an associative two-metal-aided catalytic mechanism. *J. Am. Chem. Soc.* **2008**, *130*, 10955−10962.

(12) Ivanov, I.; Tainer, J. A.; McCammon, J. A. Unraveling the three-metal-ion catalytic mechanism of the DNA repair enzyme endonuclease IV. *Proc. Natl. Acad. Sci. U. S. A.* **2007**, *104*, 1465−1470.

(13) Molina, R.; Stella, S.; Redondo, P.; Gomez, H.; Marcaida, M. J.; Orozco, M.; Prieto, J.; Montoya, G. Visualizing phosphodiester-bond hydrolysis by an endonuclease. *Nat. Struct. Mol. Biol.* **2015**, *22*, 65−72.

(14) Liao, R. Z.; Yu, J. G.; Himo, F. Phosphate mono- and diesterase activities of the trinuclear zinc enzyme nuclease P1-insights from quantum chemical calculations. *Inorg. Chem.* **2010**, *49*, 6883−6888.

(15) Samara, N. L.; Yang, W. Cation trafficking propels RNA hydrolysis. *Nat. Struct. Mol. Biol.* **2018**, *25*, 715−721.

(16) Genna, V.; Donati, E.; De Vivo, M. The Catalytic Mechanism of DNA and RNA Polymerases. *ACS Catal.* **2018**, *8*, 11103−11118.

(17) Genna, V.; Vidossich, P.; Ippoliti, E.; Carloni, P.; De Vivo, M. A Self-Activated Mechanism for Nucleic Acid Polymerization Catalyzed by DNA/RNA Polymerases. *J. Am. Chem. Soc.* **2016**, *138*, 14592−14598.

(18) Shi, Y.; Hellinga, H. W.; Beese, L. S. Interplay of catalysis, fidelity, threading, and processivity in the exo- and endonucleolytic reactions of human exonuclease I. *Proc. Natl. Acad. Sci. U. S. A.* **2017**, *114*, 6010−6015.

(19) Zhang, J.; Pan, X.; Bell, C. E. Crystal structure of lambda exonuclease in complex with DNA and Ca(2+). *Biochemistry* **2014**, *53*, 7415−7425.

(20) Zhang, J.; McCabe, K. A.; Bell, C. E. Crystal structures of lambda exonuclease in complex with DNA suggest an electrostatic ratchet mechanism for processivity. *Proc. Natl. Acad. Sci. U. S. A.* **2011**, *108*, 11872−11877.

(21) De Vivo, M.; Cavalli, A.; Carloni, P.; Recanatini, M. Computational study of the phosphoryl transfer catalyzed by a cyclin-dependent kinase. *Chem. - Eur. J.* **2007**, *13*, 8437−8444.

(22) Mulholland, A. J.; Roitberg, A. E.; Tuñón, I. Enzyme dynamics and catalysis in the mechanism of DNA polymerases. *Theor. Chem. Acc.* **2012**, *131*, 1286−1290.

(23) Genna, V.; Colombo, M.; De Vivo, M.; Marcia, M. Second-Shell Basic Residues Expand the Two-Metal-Ion Architecture of DNA and RNA Processing Enzymes. *Structure* **2018**, *26*, 40−50.

(24) Olsson, M. H.; Parson, W. W.; Warshel, A. Dynamical contributions to enzyme catalysis: critical tests of a popular hypothesis. *Chem. Rev.* **2006**, *106*, 1737−1756.

(25) Hay, S.; Scrutton, N. S. Good vibrations in enzyme-catalysed reactions. *Nat. Chem.* **2012**, *4*, 161−168.

(26) Nashine, V. C.; Hammes-Schiffer, S.; Benkovic, S. J. Coupled motions in enzyme catalysis. *Curr. Opin. Chem. Biol.* **2010**, *14*, 644−651.

(27) Garcia-Viloca, M.; Gao, J.; Karplus, M.; Truhlar, D. G. How enzymes work: analysis by modern rate theory and computer simulations. *Science* **2004**, *303*, 186−195.

(28) Pineda, J. R.; Antoniou, D.; Schwartz, S. D. Slow conformational motions that favor sub-picosecond motions important for catalysis. *J. Phys. Chem. B* **2010**, *114*, 15985−15990.

(29) Genna, V.; Carloni, P.; De Vivo, M. A Strategically Located Arg/Lys Residue Promotes Correct Base Paring During Nucleic Acid Biosynthesis in Polymerases. *J. Am. Chem. Soc.* **2018**, *140*, 3312−3321.

(30) Dreyer, J.; Brancato, G.; Ippoliti, E.; Genna, V.; De Vivo, M.; Carloni, P.; Rothlisberger, U. In *Simulating Enzyme Reactivity: Computational Methods in Enzyme Catalysis*; Tuñón, I., Moliner, V., Eds.; Royal Society of Chemistry: London, 2016; p 294.

(31) Sousa, S. F.; Fernandes, P. A.; Ramos, M. J. Computational enzymatic catalysis - clarifying enzymatic mechanisms with the help of computers. *Phys. Chem. Chem. Phys.* **2012**, *14*, 12431−12441.

(32) Senn, H. M.; Thiel, W. QM/MM Methods for Biomolecular Systems. *Angew. Chem., Int. Ed.* **2009**, *48*, 1198−1229.

(33) Kipp, D. R.; Quinn, C. M.; Fortin, P. D. Enzyme-dependent lysine deprotonation in EZH2 catalysis. *Biochemistry* **2013**, *52*, 6866−6878.

DOI: 10.1021/jacs.9b03663
J. Am. Chem. Soc. 2019, 141, 10770−10776

(34) Ishikita, H. Origin of the pKa shift of the catalytic lysine in acetoacetate decarboxylase. *FEBS Lett.* **2010**, *584*, 3464−3468.
(35) Elliott, K.; Seward, N. C.; Hampton, H.; Sumner, I. Study of the Lysine Deprotonation Mechanism in Ubiquitin Conjugating Enzyme Ubc13. *Biophys. J.* **2019**, *116*, 64a−65a.
(36) Genna, V.; Gaspari, R.; Dal Peraro, M.; De Vivo, M. Cooperative motion of a key positively charged residue and metal ions for DNA replication catalyzed by human DNA Polymerase-eta. *Nucleic Acids Res.* **2016**, *44*, 2827−2836.
(37) Kumar, K.; Woo, S. M.; Siu, T.; Cortopassi, W. A.; Duarte, F.; Paton, R. S. Cation-pi interactions in protein-ligand binding: theory and data-mining reveal different roles for lysine and arginine. *Chem. Sci.* **2018**, *9*, 2655−2665.
(38) Kumpf, R. A.; Dougherty, D. A. A mechanism for ion selectivity in potassium channels: computational studies of cation-pi interactions. *Science* **1993**, *261*, 1708−1710.
(39) Dougherty, D. A. The cation-pi interaction. *Acc. Chem. Res.* **2013**, *46*, 885−893.
(40) Gallivan, J. P.; Dougherty, D. A. Cation-pi interactions in structural biology. *Proc. Natl. Acad. Sci. U. S. A.* **1999**, *96*, 9459−9464.
(41) Ruyechan, W. T.; Olson, J. W. Surface lysine and tyrosine residues are required for interaction of the major herpes simplex virus type 1 DNA-binding protein with single-stranded DNA. *J. Virol.* **1992**, *66*, 6273−6279.
(42) Gebbie, M. A.; Wei, W.; Schrader, A. M.; Cristiani, T. R.; Dobbs, H. A.; Idso, M.; Chmelka, B. F.; Waite, J. H.; Israelachvili, J. N. Tuning underwater adhesion with cation-pi interactions. *Nat. Chem.* **2017**, *9*, 473−479.
(43) Harris, T. K.; Turner, G. J. Structural basis of perturbed pKa values of catalytic groups in enzyme active sites. *IUBMB Life* **2002**, *53*, 85−98.
(44) Isom, D. G.; Castaneda, C. A.; Cannon, B. R.; Garcia-Moreno, B. Large shifts in pK_a values of lysine residues buried inside a protein. *Proc. Natl. Acad. Sci. U.S.A.* **2011**, *108*, 5260−5265.
(45) Bordes, I.; Castillo, R.; Moliner, V. Theoretical Study of the Phosphoryl Transfer Reaction from ATP to Dha Catalyzed by DhaK from Escherichia coli. *J. Phys. Chem. B* **2017**, *121*, 8878−8892.
(46) Valiev, M.; Kawai, R.; Adams, J. A.; Weare, J. H. The role of the putative catalytic base in the phosphoryl transfer reaction in a protein kinase: first-principles calculations. *J. Am. Chem. Soc.* **2003**, *125*, 9926−9927.
(47) Murillo-López, J.; Zinovjev, K.; Pereira, H.; Caniuguir, A.; Garratt, R.; Babul, J.; Recabarren, R.; Alzate-Morales, J.; Caballero, J.; Tuñón, I.; Cabrera, R. Studying the phosphoryl transfer mechanism of the *E. coli* phosphofructokinase-2: from X-ray structure to quantum mechanics/molecular mechanics simulations. *Chem. Sci.* **2019**, *10*, 2882−2892.
(48) Matute, R. A.; Yoon, H.; Warshel, A. Exploring the mechanism of DNA polymerases by analyzing the effect of mutations of active site acidic groups in Polymerase. *Proteins: Struct., Funct., Genet.* **2016**, *84*, 1644−1657.
(49) Tse, C. K. M.; Xu, J.; Xu, L.; Sheong, F. K.; Wang, S.; Chow, H. H.; Gao, X.; Li, X.; Cheung, P. P.; Wang, D.; Zhang, Y.; Huang, X. Intrinsic cleavage of RNA polymerase II adopts a nucleobase-independent mechanism assisted by transcript phosphate. *Nat. Catal.* **2019**, *2*, 228−235.
(50) Kennedy, C. R.; Lin, S.; Jacobsen, E. N. The Cation-pi Interaction in Small-Molecule Catalysis. *Angew. Chem., Int. Ed.* **2016**, *55*, 12596−12624.
(51) Grimme, S. Accurate description of van der Waals complexes by density functional theory including empirical corrections. *J. Comput. Chem.* **2004**, *25*, 1463−1473.
(52) Lin, I. C.; Coutinho-Neto, M. D.; Felsenheimer, C.; von Lilienfeld, O. A.; Tavernelli, I.; Rothlisberger, U. Library of dispersion-corrected atom-centered potentials for generalized gradient approximation functionals: Elements H, C, N, O, He, Ne, Ar, and Kr. *Phys. Rev. B: Condens. Matter Mater. Phys.* **2007**, *75*, 205131.
(53) Mitsis, P. G.; Kwagh, J. G. Characterization of the interaction of lambda exonuclease with the ends of DNA. *Nucleic Acids Res.* **1999**, *27*, 3057−3063.
(54) van Oijen, A. M.; Blainey, P. C.; Crampton, D. J.; Richardons, C. C.; Ellenberger, T.; Xie, X. S. Single-Molecule Kinetics of lambda exonuclease Reveal Base Dependence and Dynamic Disorder. *Science* **2003**, *301*, 1235−1238.
(55) Torrie, G. M.; Valleau, J. P. Nonphysical sampling distributions in Monte Carlo free-energy estimation: Umbrella sampling. *J. Comput. Phys.* **1977**, *23*, 187−199.
(56) Kumar, S.; Bouzida, D.; Swendsen, R. H.; Kollman, P. A.; Rosenberg, J. M. THE weighted histogram analysis method for free-energy calculations on biomolecules. I. The method. *J. Comput. Chem.* **1992**, *13*, 1011−1021.
(57) Wang, L.; Li, L.; Alexov, E. pKa predictions for proteins, RNAs, and DNAs with the Gaussian dielectric function using DelPhi pKa. *Proteins: Struct., Funct., Genet.* **2015**, *83*, 2186−2197.
(58) Wang, L.; Zhang, M.; Alexov, E. DelPhiPKa web server: predicting pKa of proteins, RNAs and DNAs. *Bioinformatics* **2016**, *32*, 614−615.
(59) Ruan, C.; Yang, Z.; Hallowita, N.; Rodgers, M. T. Cation-pi interactions with a model for the side chain of tryptophan: structures and absolute binding energies of alkali metal cation-indole complexes. *J. Phys. Chem. A* **2005**, *109*, 11539−11550.
(60) Ma, J. C.; Dougherty, D. A. The Cation-pi Interaction. *Chem. Rev.* **1997**, *97*, 1303−1324.
(61) Biertumpfel, C.; Yang, W.; Suck, D. Crystal structure of T4 endonuclease VII resolving a Holliday junction. *Nature* **2007**, *449*, 616−620.
(62) Liang, G.; Webster, C. E. Phosphoramidate hydrolysis catalyzed by human histidine triad nucleotide binding protein 1 (hHint1): a cluster-model DFT computational study. *Org. Biomol. Chem.* **2017**, *15*, 8661−8668.
(63) Yoon, H. Z.; Zhao, L. N.; Warshel, A. Exploring the catalytic mechanism of Cas9 using information inferred from Endonuclease VII. *ACS Catal.* **2019**, *9*, 1329−1336.
(64) Zuo, Z.; Liu, J. Structure and Dynamics of Cas9 HNH Domain Catalytic State. *Sci. Rep.* **2017**, *7*, 17271.
(65) Li, C. L.; Hor, L. I.; Chang, Z. F.; Tsai, L. C.; Yang, W. Z.; Yuan, H. S. DNA binding and cleavage by the periplasmic nuclease Vvn: a novel structure with a known active site. *EMBO J.* **2003**, *22*, 4014−4025.
(66) Jinek, M.; Jiang, F.; Taylor, D. W.; Sternberg, S. H.; Kaya, E.; Ma, E.; Anders, C.; Hauer, M.; Zhou, K.; Lin, S.; Kaplan, M.; Iavarone, A. T.; Charpentier, E.; Nogales, E.; Doudna, J. A. Structures of Cas9 endonucleases reveal RNA-mediated conformational activation. *Science* **2014**, *343*, 1247997.
(67) Palermo, G.; Miao, Y.; Walker, R. C.; Jinek, M.; McCammon, J. A. CRISPR-Cas9 conformational activation as elucidated from enhanced molecular simulations. *Proc. Natl. Acad. Sci. U. S. A.* **2017**, *114*, 7260−7265.
(68) Palermo, G. Structure and Dynamics of the CRISPR-Cas9 Catalytic Complex. *J. Chem. Inf. Model.* **2019**, *59*, 2394−2406.
(69) Jiang, F.; Taylor, D. W.; Chen, J. S.; Kornfeld, J. E.; Zhou, K.; Thompson, A. J.; Nogales, E.; Doudna, J. A. Structures of a CRISPR-Cas9 R-loop complex primed for DNA cleavage. *Science* **2016**, *351*, 867−871.
(70) Huai, C.; Li, G.; Yao, R.; Zhang, Y.; Cao, M.; Kong, L.; Jia, C.; Yuan, H.; Chen, H.; Lu, D.; Huang, Q. Structural insights into DNA cleavage activation of CRISPR-Cas9 system. *Nat. Commun.* **2017**, *8*, 1375.
(71) Zhang, F.; Gao, L.; Zetsche, B.; Slaymaker, I. *CRISPR enzyme mutations reducing off-target effects*; PCT/US2016/038034, The Broad Institute Inc., Massachusetts Institute of Technology (M.I.T.), 2016.
(72) Arangundy-Franklin, S.; Taylor, A. I.; Porebski, B. T.; Genna, V.; Peak-Chew, S.; Vaisman, A.; Woodgate, R.; Orozco, M.; Holliger, P. A synthetic genetic polymer with an uncharged backbone chemistry based on alkyl phosphonate nucleic acids. *Nat. Chem.* **2019**, *11*, 533−542.

DOI: 10.1021/jacs.9b03663
J. Am. Chem. Soc. 2019, 141, 10770−10776